Second-order filter-based inertia emulation (SOFIE) for low inertia power systems—Part 1: Principles and Equivalence with Synchronous Machine

Journal:	*IEEE Transactions on Power Delivery*
Manuscript ID	TPWRD-01181-2022
Manuscript Type:	Special issue: Advances in Research and Applications of Power Electronics in T&D Systems
Date Submitted by the Author:	07-Aug-2022
Complete List of Authors:	Aragón Sotelo, Diego; Tecnalia, Energy and Environment Division; university of mondragon, Unamuno, Eneko; Mondragon Unibertsitatea, Electronics and Computing Department Gil de Muro, Asier; Tecnalia Research and Innovation Ceballos, Salvador; Tecnalia Research and Innovation, Barrena, Jon Andoni; University of Mondragon, Computing and Electronics
Technical Topic Area :	grid-connected converter control
Key Words:	Grid-supporting control, Second-order low-pass filter, Small signal analysis, Synchronous machine

Second-order filter-based inertia emulation (SOFIE) for low inertia power systems—Part 1: Principles and Equivalence with Synchronous Machines

D. A. Aragon*, E. Unamuno, A. Gil de Muro, S. Ceballos, J. A. Barrena

***Abstract*—The massive integration of power electronic converters into the power grid has led to a decrease in the mechanical inertia of the power system, causing an increase in the rate of change of frequency (RoCoF) that may lead to stability problems. The scientific community has focused on developing grid-forming control techniques, although their implementation implies a significant change in the firmware of the converter. Grid-supporting approaches, on the other hand, are an interesting alternative to add frequency support to the grid while preserving the original control structure of the converter. This paper proposes three new grid-supporting control techniques based on the dynamic behaviour of a synchronous machine (SM) and its equivalence with a second-order low-pass filter. They endow the converter with the capability of providing synthetic inertia, damping, droop-based *p/f* primary response and virtual reactance. The dynamics of the proposed implementations are compared with those of a reduced-order synchronous machine by means of time-domain simulations and in-depth state-space based small signal analyses. Besides, their operation is validated in a nine-bus low-inertia power system. Hardware in the loop (HIL) laboratory results are used to validate experimentally the proposed techniques.**

***Index Terms*—Grid-supporting control, Second-order low-pass filter, Small signal analysis, Synchronous machine.**

I. Introduction

The ambitious goal of reducing greenhouse gas emissions has set in motion an accelerated integration of non-conventional renewable energies (nRES) into the electricity grid, forecasting that by 2050 the 86% of electricity generated will be supplied by renewable sources [1]. Most nRES are connected to the power grid using electronic power converters, which are synchronised with the grid with phase-locked loop (PLL) algorithms [2]. These devices are known as grid-following (GFL) because they do not contribute to the frequency and voltage regulation of the grid. The replacement of conventional generation based on synchronous machines (SM) with this type of nRES leads to a reduction of the mechanical inertia connected to the grid, degrading the stability of the power system [3]. Moreover, the stochastic nature of these sources leads to highly variable generation profiles, impacting directly on the system power balance. To overcome these challenges, nRES are usually integrated in the grid with energy storage systems (ESS), and are controlled as grid-forming (GFM) or grid-supporting (GSC) devices to provide frequency and voltage support [4].

The advantage of GFM is that the converter operates as a voltage source and is capable of generating the voltage waveform without using a PLL. This type of devices are specially relevant at power systems with a 100% penetration of converter-interfaced devices where nRES and ESS have replaced all the conventional synchronous generation. In the literature, several implementations of GFM proposals can be found, such as the ones based on droop control [5], synchronous machine emulation [6], [7], virtual oscillators [8] or matching control [9]. A comparative evaluation of some of these control strategies can be also found in [10].

GSCs, on the other hand, perform as current sources and are not capable of forming the grid by themselves, but they are an interesting alternative because they can provide frequency support with minimal modifications in the original controller. Broadly speaking, GSCs can be categorised in two different groups: droop-based and inertia emulation. Both approaches employ a PLL for synchronisation and internal loops to regulate the output current [2]. In droop-based GSCs, the frequency support is provided by injecting active power proportionally to the deviation of the frequency, following a *p/f* droop characteristic. This approach is simple and easily implementable, but its dynamic response against power perturbations highly depends on the dynamics of the PLL [11] and it does not provide inertial support. In inertia emulation GSCs, the active power injections are proportional to the rate of change of the frequency (RoCoF or $d\omega/dt$), thus providing synthetic inertia. Nonetheless, their main disadvantages are that the derivative term make them susceptible to the noise of the estimated frequency and the system response is strongly linked to the dynamics of the PLL [12]. Some authors try to overcome these challenges by using a first-order low-pass filter at the estimated frequency [13] or by replacing the derivative with a first-order wash-out filter [14].

Unlike GFMs that are capable of emulating effectively the behaviour of a SM, the main problem of GSCs is that their dynamic operation under power perturbations deviates from the expected behaviour of a SM. The first-order filter adopted to cope with sudden frequency variations does not provide a response equivalent to the well-known swing equation. Besides, some authors have reported stability problems due to adverse interactions induced by the first-order low-pass filter

This work has been partially funded by the Basque Government under the project EP4H2 (KK-2022/00039).

*Corresponding author (e-mail: diego.aragon@tecnalia.com)

D. A. Aragon, A. Gil de Muro and S. Ceballos are with Tecnalia, Basque Research and Technology Alliance (BRTA), Parque Tecnológico de Bizkaia, 48160 Derio, Spain

E. Unamuno and J. A. Barrena are with the Electronics and Computing Department, Mondragon Unibertsitatea, 20500 Arrasate-Mondragón, Spain

inertia control and the *LC* resonances of the power system [12], [13]. As a solution, a proposal is to slow down the PLL dynamics to avoid strong transients [13], but this modification affects the converter synchronisation and its voltage regulation. Recently, the so-called external inertial emulation technique has been proposed to approximate the response of GSCs to that of SMs [15]. It consists of an external control based on the swing equation that provides an active power reference to a traditional GFL control structure. However, there have been no studies of the impact of the PLL or a detailed analysis of its equivalence to a synchronous machine.

Motivated by the need to overcome the previous issues, this work proposes an alternative GSC controller named second-order filter-based inertia emulation (SOFIE). As the name suggests, this control technique is based on an equivalence between a second-order low-pass filter and the reduced model of a classical SM. Its main features and novelties with regards to previous GSCs are:

1) Reproducing accurately the main dynamics defined by the swing-equation of SMs on which frequency stability relies.
2) Solving the stability problems of traditional first-order filter-based inertia emulation techniques, which are caused by the interactions of the GSC control with the *LC* resonances of the power system. This aspect is discussed thoroughly in [16].
3) Providing fully independent and configurable virtual inertia constant, droop and damping gains, and virtual inductance.
4) Facilitating the seamless integration with existing GFL controllers. State-of-the-art inertia emulation algorithms based on derivative terms can quickly adopt the proposed technique by replacing the first-order filter with a second-order one. These facts enable the conversion/upgrade of existing converters already in use to accurately reproduce the dynamics of SMs.
5) Providing virtual damping to attenuate power oscillations without affecting the steady-state value of the frequency.
6) Decoupling PLL dynamics with inertia emulation control, allowing fast PLLs without compromising the system stability.

The rest of the paper is structured as follows: Section II introduces the principles and analytical derivation of three different SOFIE control variants. Section III evaluates their time-domain operation and carries out a modal analysis to characterise them. Section IV introduces a parametric sensitivity analysis of the proposed techniques, while Section V evaluates the influence of the PLL on their performance. Section VI compares the performance of the proposed control against a SM in a low inertia grid. Finally, Section VII provides experimental validation with a real-time HIL system and Section VIII concludes the paper.

II. Principles and analytical derivation of the SOFIE control

The purpose of this section is to lay the foundations of the proposed SOFIE technique, which is based on an equivalence between the simplified model of a SM and a second-order filter. Initially, the swing equation that represents the electromechanical response of a synchronous generator is described, as it is the basis of the proposed control philosophy. Then, the analytical rationale behind the proposed technique is described, and three different SOFIE control variants are proposed. The last subsection introduces how to incorporate these variants in the typical control structure of a power converter.

A. Simplified synchronous machine

The generator model taken as a basis for the proposed control techniques is based on a simplified electromechanical model of a SM, which is driven by a turbine whose governor is controlled by an active power control (APC). It must be noted that in the following the response of the governor and the turbine is assumed to be instantaneous—i.e., no delay is considered in their response.

The dynamic equation describing the time evolution of the angular speed of the rotor using per unit notation and assuming that $\omega_r \approx 1$ p.u. is given by [17]:

$$\dot{\omega_r} = \frac{p_m - p_e - k_d\left(\omega - \omega_g\right)}{2H} \tag{1}$$

where p_e and p_m are the electrical and mechanical power, respectively. k_d is the damping constant, H is the inertia constant and ω_g is the frequency at the machine terminals. The mechanical speed of the rotor ω_r is related to the electrical speed of the induced electromotive force (ω) through the number of pole pairs (p_l) as $\omega = \omega_r p_l$. To simplify the notation and without loss of generality, in the rest of the paper the system is considered to have a single pair of poles, thus $\omega = \omega_r$.

Since no delays are considered in the turbine and the governor, the mechanical power is set by the APC, which is comprised by a p/f droop control described as:

$$p_m = p^* + k_\omega\left(\omega^* - \omega\right) \tag{2}$$

where p^* and ω^* are the output power and grid frequency setpoints, respectively, and k_ω is the droop constant.

The stator winding of a SM can be modelled as a series *RL* impedance. The current through that winding can be represented by the following differential equation:

$$\mathbf{i}_s = \frac{\omega_b}{L_s}\left[\mathbf{e}_s - \mathbf{v_o} - \left(R_s + j\,\omega L_s\right)\mathbf{i}_s\right] \tag{3}$$

where $\mathbf{i}_s$ is the stator current represented in a *dq* reference frame using a vector notation ($\mathbf{i}_s = i_d + j i_q$). $\mathbf{v}_o$ is the voltage at the point of common connection (PCC), and L_s and R_s are the inductance and armature resistance, respectively. $\mathbf{e}_s$ is the vector representing the internal voltage of the generator.

The electrical power that the SM exchanges with the grid can be expressed in a simplified manner by [17]:

$$p_e = \frac{|\mathbf{e}_s|\,|\mathbf{v}_o|}{X_s}\sin\delta \tag{4}$$

where $X_s = \omega L_s$ and δ is the angle difference between $\mathbf{e}_s$ and $\mathbf{v}_o$. This angle difference can be calculated from the SM electrical frequency and the grid-side frequency as:

$$\dot{\delta} = \omega_b \left(\omega - \omega_g\right) \tag{5}$$

where ω_b is the base angular frequency used in per unit notation.

When the angle difference is very small, $\sin\delta \approx \delta$. Moreover, when assuming that in per unit $\mathbf{e}_s \approx \mathbf{v}_o \approx 1$ p.u., Eq. (4) can be linearised around an operating point as:

$$p_e \approx \frac{1}{X_s}\delta \tag{6}$$

Eqs. (1), (2), (5), and (6) constitute the state-space model that represent the electromechanical motion of a SM. Taking the Laplace transformation of these expressions and after some manipulations, the following transfer function can be defined:

$$p_e\,(s) = G_1\,(s)p^* + G_2\,(s)\omega^* + G_3\,(s)\omega_g\,(s) \tag{7}$$

where $G_1\,(s)$, $G_2\,(s)$ and $G_3\,(s)$ are defined as:

$$G_1\,(s) = \frac{\omega_b}{2HX_s\left(s^2 + \dfrac{(k_d + k_\omega)s}{2H} + \dfrac{\omega_b}{2HX_s}\right)} \tag{8}$$

$$G_2\,(s) = \frac{\omega_b\, k_\omega}{2HX_s\left(s^2 + \dfrac{(k_d + k_\omega)s}{2H} + \dfrac{\omega_b}{2HX_s}\right)} \tag{9}$$

$$G_3\,(s) = \frac{-\dfrac{\omega_b\, s}{X_s} - \dfrac{\omega_b\, k_\omega}{2HX_s}}{s^2 + \dfrac{(k_d + k_\omega)}{2H}s + \dfrac{\omega_b}{2HX_s}} \tag{10}$$

B. Introducing the SOFIE controllers

Assuming that the internal power control of a converter is very fast (i.e., that $p_e \approx p_e^*$), the dynamic response of a classical inertia emulation GSC can be represented by the following transfer function [12], [13]:

$$p_e\,(s) = -2\,H\,\frac{\omega_n\, s}{s + \omega_n}\,\omega_g\,(s) + k_\omega\,\left(\omega^* - \omega_g\,(s)\right) + p^* \tag{11}$$

where ω_n is the cutoff frequency of the first-order low-pass filter used to avoid sudden frequency variations. The value of this low-pass filter is then passed through a derivative term to emulate an inertial behaviour. Moreover, a droop controller with gain k_ω is provided to simultaneously carry out the primary regulation and to damp the output response, meaning that droop and damping terms are not decoupled [18], [19]. These characteristics cause the dynamic response of this type of control to differ significantly from the behaviour expected from a simplified SM. This can be also concluded from the differences observed between Eqs. (7)–(10) and Eq. (11).

The purpose of the SOFIE control is to approximate the behaviour of a power converter to that of a simplified SM, but without the need to modify the original control structure as it is done in other SM emulation techniques. For that purpose, the first-order filter used in the power control of classical inertia emulation techniques is replaced by a second-order low-pass filter. In this way the dynamic response of a converter controlled with a SOFIE technique will be more similar to the one observed in Eqs. (7)–(10).

Fig. 1 shows three different implementations of the SOFIE technique. Below their equivalent transfer functions are analysed to illustrate the similarities compared to Eqs. (7)–(10).

The first implementation, named SOFIE 1, is formed by replacing the first-order filter in Eq. (11) by a second-order filter. Based on the diagram depicted in Fig. 1(a) and following the notation in Eq. (7), the equivalent transfer functions that represent the electrical power (p_e) provided by converters controlled with this technique are:

$$G_1\,(s) = 1 \tag{12}$$

$$G_2\,(s) = k_\omega \tag{13}$$

$$G_3\,(s) = \frac{-k_\omega s^2 + (2H\omega_n^2 - 2k_\omega\omega_n\zeta_v)s - k_\omega\omega_n^2}{s^2 + 2\omega_n\zeta_v s + \omega_n^2} \tag{14}$$

The denominator of Eq. (14) has the same order as that of the simplified SM in Eq. (10). Therefore, the natural frequency (ω_n) and damping term (ζ_v) of the second-order filter in Eq. (14) can be defined as:

$$\omega_n = \sqrt{\frac{\omega_b}{2HX_s}} \tag{15}$$

$$\zeta_v = \frac{(k_d + k_\omega)\sqrt{2}}{4\sqrt{\dfrac{\omega_b\, H}{Xs}}} \tag{16}$$

Note how ω_n and ζ_v can be designed as a function of SM parameters to provide a response similar to a simplified SM under grid-side frequency variations (ω_g). Replacing (15) and (16) into (12)–(14), the following transfer functions are obtained:

$$G_1\,(s) = 1 \tag{17}$$

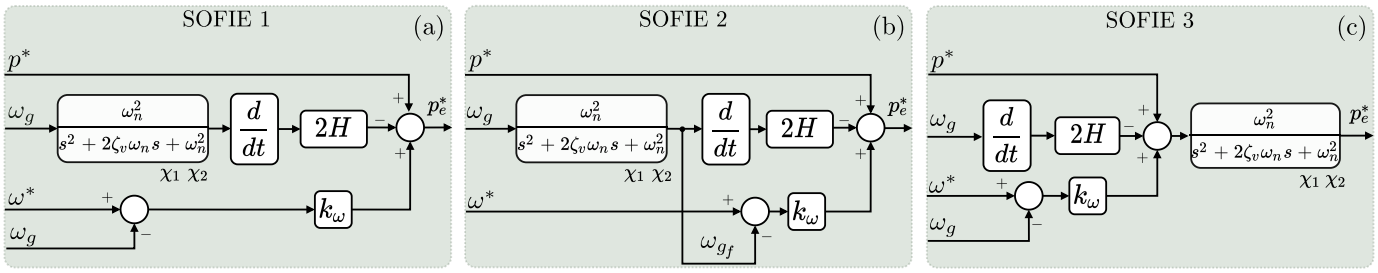

Fig. 1. Proposed SOFIE variants.

$$G_2(s) = k_\omega \tag{18}$$

$$G_3(s) = \frac{-k_\omega s^2 + \left(-\frac{\omega_b}{X_s} - \frac{k_\omega (k_d + k_\omega)}{2H}\right) s - \frac{k_\omega \omega_b}{2HX_s}}{s^2 + \frac{(k_d + k_\omega)}{2H} s + \frac{\omega_b}{2HX_s}} \tag{19}$$

Comparing Eqs. (19) and (10), one can conclude that the dynamics of the SOFIE 1 controller, defined by the poles of (19), are the same than those of the swing-equation in Eq. (10). However, the zeros of both transfer functions are different, meaning that SOFIE 1 approximates the electromechanical response of a synchronous machine in the presence of frequency variations but does not completely match it due to the divergence in the zeros. Besides, the dynamic response of SOFIE 1 under power or frequency reference variations—given by Eqs. (17) and (18), respectively—differ from those defined in Eqs. (8) and (9). In this sense, it can be concluded that SOFIE 1 can provide emulated inertia against frequency changes, but it does not provide an accurate representation of a synchronous machine.

Fig. 1(b) shows a second implementation (SOFIE 2), where the second-order filter also operates over the frequency input used to implement the droop controller. Following the same reasoning as in the previous case, and making use of Eqs. (15) and (16), the transfer functions that define the response of SOFIE 2 take the form given by Eq. (7), where:

$$G_1(s) = 1 \tag{20}$$

$$G_2(s) = k_\omega \tag{21}$$

$$G_3(s) = \frac{-\frac{\omega_b s}{X_s} - \frac{\omega_b k_\omega}{2HX_s}}{s^2 + \frac{(k_d + k_\omega)}{2H} s + \frac{\omega_b}{2HX_s}} \tag{22}$$

Eqs. (22) and (10) are now identical since they have the same zeros and poles. Hence, one can conclude that the response provided by SOFIE 2 to frequency changes in the grid replicates with accuracy that of the simplified model of the SM. The electrical power injected in the grid by the SOFIE 2 controller to respond against variations in the grid frequency emulates the electrical power of an equivalent synchronous machine with a defined inertia, impedance, and droop and damping gains. However, Eqs. (20) and (21) are different from (8) and (9), indicating that the response of SOFIE 2 to changes in the power or frequency references does not match that of a SM.

In the third implementation, named SOFIE 3, the second-order filter operates over the electrical power reference instead of only over the grid frequency (Fig. 1(c)). The transfer functions that determine the dynamic response of SOFIE 3, provided that the equivalences in Eqs. (15) and (16) are used, takes the same form as Eq. (7), where:

$$G_1(s) = \frac{\omega_b}{2HX\left(s^2 + \frac{(k_d + k_\omega)s}{2H} + \frac{\omega_b}{2HX}\right)} \tag{23}$$

$$G_2(s) = \frac{\omega_b k_\omega}{2HX_s\left(s^2 + \frac{(k_d + k_\omega)s}{2H} + \frac{\omega_b}{2HX_s}\right)} \tag{24}$$

$$G_3(s) = \frac{-\frac{\omega_b s}{X_s} - \frac{\omega_b k_\omega}{2HX_s}}{s^2 + \frac{(k_d + k_\omega)}{2H} s + \frac{\omega_b}{2HX_s}} \tag{25}$$

In the SOFIE 3 implementation, Eqs. (23)–(25) are identical to (8)–(10), so it can be concluded that this controller provides a response that matches that of the simplified SM model under variations in the grid frequency, the reference power and the reference frequency.

Among the proposed implementations, SOFIE 3 is the approach that most accurately replicates the response of a simplified SM. Nevertheless, its implementation implies a slight variation on the structure of classical inertia emulation techniques as the filter does not only operate on the grid frequency. SOFIE 2 is an interesting approach because it achieves the same dynamic response as SMs under grid frequency variations by providing synthetic inertia, while it responses instantaneously to changes in the power and frequency set-points set by the plant operator or a higher level controller. SOFIE 1 requires almost no variation on the structure of classical inertia emulation controllers. However, it replicates the operation of SMs with a minor degree of accuracy.

C. Integration of SOFIE controllers in the control structure of a grid-connected converter

The diagram in Fig. 2 illustrates how SOFIE controllers can be integrated within the typical structure of a grid-connected converter developed in the *dq* synchronous reference frame. This controller basically consists of PI regulators to control the current, including the coupling terms (k_{xc}) and feed-forward terms (k_{ffv}). As depicted in Fig. 1, the output of SOFIE controllers is the electrical power reference of the converter (p_e^*), which is converted into current set-points ($\mathbf{i}_c^*$) taking into account the measured terminal voltage ($\mathbf{v}_o$). Consequently, the integration with the inner converter control loops is seamless. The integration with other control implementations on the natural or stationary reference frame is also possible, since SOFIE controllers are agnostic of the structure of the inner control loops.

It is also convenient to remark that the frequency of the grid that is used as an input to the SOFIE controller is estimated using a classical synchronous reference frame PLL. The transfer functions of the SOFIE controllers in the previous section have been obtained neglecting the dynamics of the PLL and the inner current control loops. However, they will play a role in the final dynamic response of the converter. The effect of synchronisation algorithms in the dynamic response is usually neglected in the literature related to GSC, so this aspect is addressed in the following sections.

III. Time-domain performance of SOFIE control

The aim of this section is to corroborate the hypotheses made in the analytical description of the three SOFIE implementations. For that purpose, initially the testing scenario is described, and then the performance of the controllers is evaluated by providing the time-domain response under

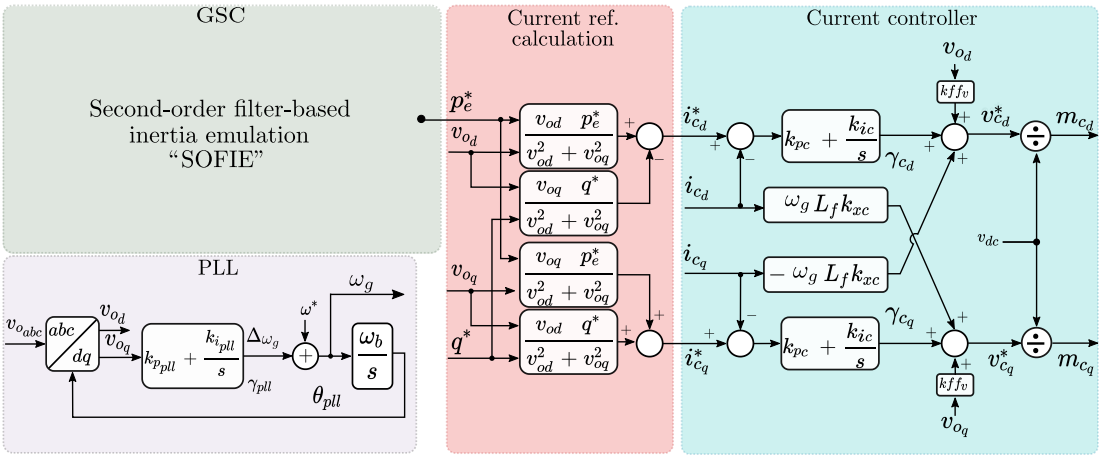

Fig. 2. Control structure of the converter.

various disturbances and by comparing the system modes of oscillation. The simplified model of a SM is taken as the benchmark system.

A. Description of the testing scenario

Since the SOFIE controller is a GSC, another grid-connected device must be responsible for setting the grid voltage and frequency. In this case, the testing scenario shown in Fig. 3 consists of an inverter with a series inductive filter (L_f) connected to an infinite bus via an inductive transmission line (L_g). A small resistance, accounting for the line and filter losses, has been considered as well.

The configuration employed to obtain the results of the simplified SM model is the same as the one shown in Fig. 3, but the inverter and its filter is replaced by the SM modelled in II-A.

The parameters and set-points employed in the following tests are gathered in Appendix A. The control parameters of the SOFIE controllers (i.e., $\omega_n, \zeta_v,$) are calculated using Eqs. (15) and (16), and taking the SM parameters as a reference. The modulus optimum criterion technique is used to tune the current PI regulators [20]. Moreover, the PLL is tuned employing the symmetric optimal criterion technique to ensure the maximum phase margin at the crossover frequency of the open-loop transfer function [21].

B. Performance tests

1) Active power reference variation: Fig. 4 depicts the behaviour of the electrical system described in Fig. 3 under a step-shaped variation of 0.1 p.u. in the active power reference (p^*) of the SOFIE implementations and the simplified SM model at t = 1s.

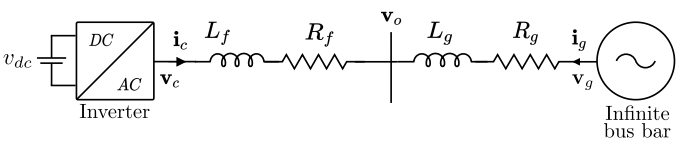

Fig. 3. Testing scenario: power converter connected to an infinite grid model.

The results show that the dynamic response of SOFIE 1 and SOFIE 2 implementations is significantly faster than that of the SOFIE 3 implementation and the SM. As stated in Section II-B, the reason is that the power reference is not being filtered in SOFIE 1 and 2 (refer to Fig. 1). However, under the power set-point variation, the SOFIE 3 implementation emulates the behaviour of the SM very closely, confirming the hypothesis made with the equivalent Eqs. (23)–(25).

2) Grid frequency variation: The behaviour under grid-side frequency variations is studied by making a step-shaped change of -0.01 p.u. in the infinite bus frequency at t = 1s. Fig. 5 shows the time-domain evolution of the active power supplied by the SOFIE implementations and the SM.

The active power in the steady state takes the same value for all the cases; this makes sense as it only depends on the droop gain k_ω. Regarding the transient response, all the systems have similar behaviour, but SOFIE 1 exhibits a faster transient response and a higher overshoot. This is due to the fact that the second-order filter is not applied to the frequency term used in the *p/f* droop curve, which is directly driven by frequency estimated by the PLL. This overshoot is not observed in SOFIE 2 and SOFIE 3 implementations as the estimated frequency is filtered before applying the droop characteristic and the derivative term. Consequently, the dynamic behaviour of SOFIE 2 and SOFIE 3 matches very well the response expected from a SM.

The time-domain results provided in these two sections

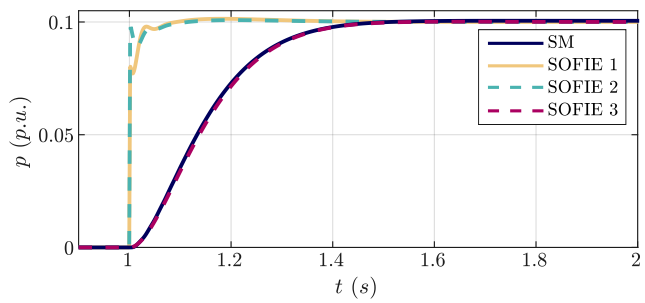

Fig. 4. Active power for a 0.1 p.u. variation in the power reference (p^*)

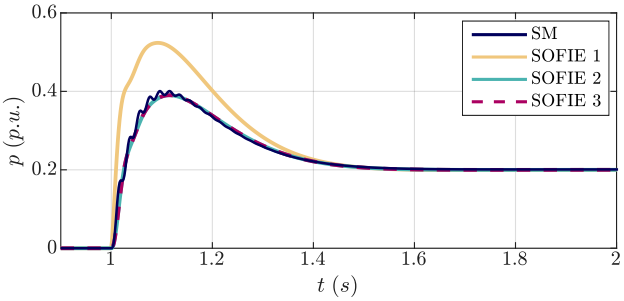

Fig. 5. Active power for a -0.01 p.u. variation in the grid frequency (ω_g)

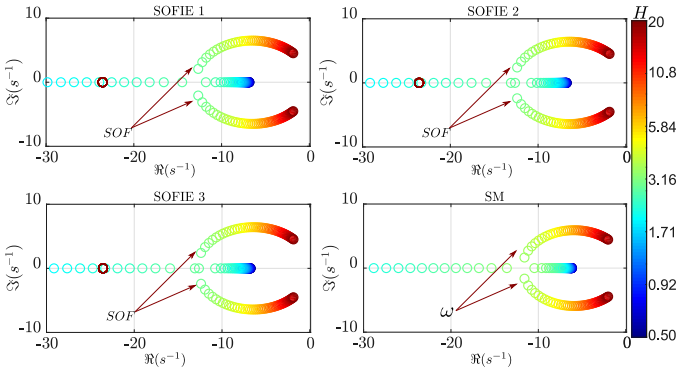

Fig. 6. Root-locus under a variation of the inertia constant (H).

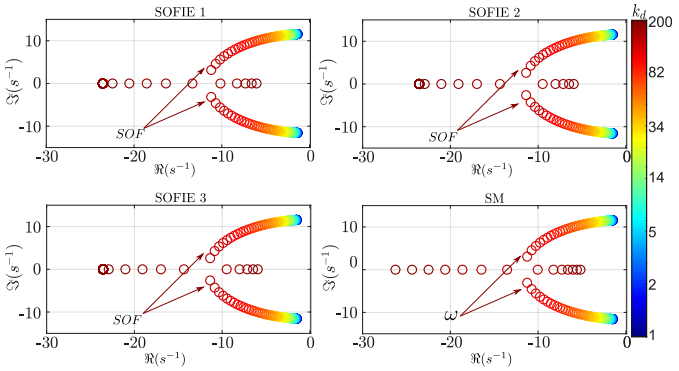

Fig. 7. Root-locus under a variation of the damping gain (k_d).

demonstrate that, even if the SOFIE controller depends on a synchronisation algorithm such as a PLL to synchronise with the grid, their transient behaviour can be designed to be equivalent to the simplified model of a SM.

IV. Parametric sensitivity analysis

This section further evaluates how the variation of several physical or control parameters influences the location of eigenvalues of the proposed SOFIE controllers in the complex plane. The analysis will help to identify the similarities between the SOFIE implementations and the SM. To make the analysis, a state-space representation of the SOFIE controllers has been made and their eigenvalues are computed by making use of the CSTEP tool introduced in [22].

A. Inertia constant (H) variation

Fig. 6 shows the location of the electromechanical eigenvalues in the complex plane for the three SOFIE implementations (SOF) and the SM machine (ω), as the value of the inertia constant H changes. The eigenvalues move almost identically in the four cases, corroborating once again the similarities in the behaviour of the proposed SOFIE controllers and the SM.

For low inertia constants, the eigenvalues are real, revealing a non-oscillatory nature of the electromechanical modes. However, as the inertia increases, the poles describe a circumference with diameter $(2\,\omega_b)/((k_d + k_\omega)\,X_s)$. Consequently, as H increases the eigenvalues become complex numbers and the electromechanical modes exhibit an under-damped oscillatory behaviour. The damping factor of the modes decreases as H increases.

B. Damping constant (k_d) variation

Fig. 7 shows the root locus for the damping gain parametric sweep. As k_d increases the electromechanical eigenvalues describe a semi-circumference with centre at the origin and radius equal to the natural frequency (16). This tendency continues until a threshold point is reached where the eigenvalues become real. For the proposed case study, this threshold value is $k_d = 151$. Results shows that for $k_d < 151$ the damping factor of the electromechanical eigenvalues of the SM and the SOFIE implementations is lower than 1, resulting in an under-damped system. For all the implementations, the imaginary part of the electromechanical eigenvalues decreases as k_d increases. For $k_d > 151$, the damping factor becomes $\zeta > 1$, thus the eigenvalues associated to the electromechanical response become real and begin to separate from each other in the real axis. These results illustrates how, for high values of emulated inertia H, the damping gain k_d of the SOFIE controllers can be properly adjusted to increase the damping of the electromechanical modes.

C. Droop constant (k_ω) variation

The analysis of the droop constant is fundamental because it determines how active power is shared among the devices participating in the frequency regulation of the grid. Its value is usually defined according to the maximum power of the device and the critical frequency boundaries established by the grid operator. Depending on the value of this droop constant, a converter might be constrained to work in certain operation conditions because it might cause undesired oscillations or instabilities. It can be observed in the zoomed regions of Fig. 8 that the electromechanical eigenvalues of the SOFIE controllers and those of the SM exhibit a similar behaviour as k_ω is swept, thus certifying that the SOFIE implementation approximates the dynamic response of SMs. As k_ω increases, the damping factor of the electromechanical modes increases as well. This behaviour is similar to that exhibited in Fig. 7 when k_d increased, being possible to conclude that in the proposed SOFIE controllers, the damping and droop gains play an equivalent role in defining the damping factor. This is aligned with the analytical expression of the damping

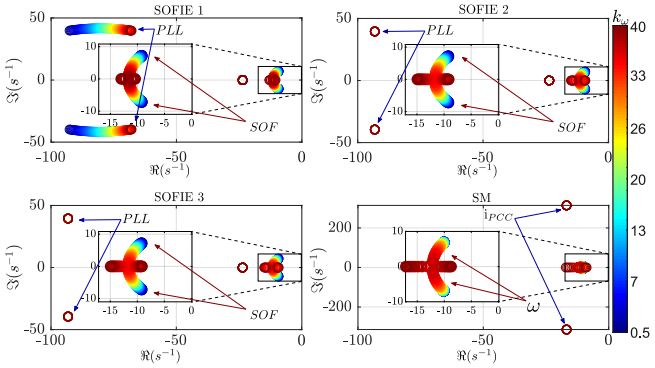

Fig. 8. Root-locus under a variation of the droop gain (k_ω).

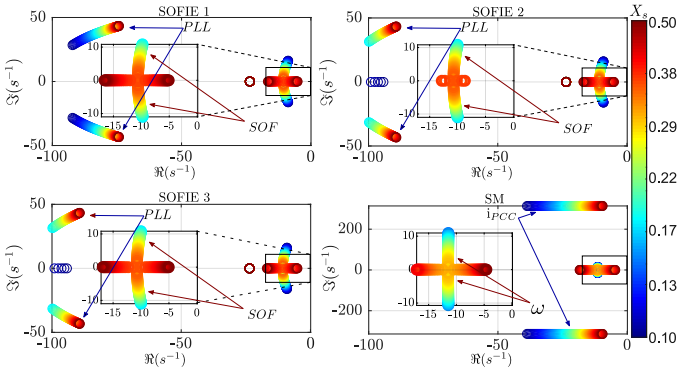

Fig. 9. Root-locus under a variation of the virtual reactance (X_s).

factor provided in (16). However, it is important to note that, while the droop gain modifies the point of operation of the converter in steady-state (because it is a proportional gain), the damping term only reacts under frequency variations ($\Delta\omega$), and therefore it should not cause a steady-state deviation.

In addition, the eigenvalues with high participation factor of the PLL state variables are also displayed in Fig. 8. While in the SOFIE 2 and 3 the variation of the droop gain does not have any influence in their location, in SOFIE 1 the attenuation constant of these eigenvalues decreases (the eigenvalues move towards the right half plane) as the droop gain increases. Therefore, it takes more time to damp these oscillatory modes. This is due to the fact that the dynamic response of the droop loop in SOFIE 1 is directly coupled to the PLL because the estimated frequency is not filtered.

D. Series reactance (X_s) variation

The influence of a variation of the virtual series reactance of SOFIE implementations and the SM stator reactance are shown in Fig. 9.

It can be observed in the zoomed regions of Fig. 9 that, as the virtual reactance increases, the electromechanical modes of the three SOFIE implementations and those of the SM move towards the real axis of the complex plane, thus becoming more damped. This is aligned with the analytical expression found for the damping factor in (16). Above a threshold value of the virtual reactance, the damping factor becomes higher than 1 and the electromechanical modes become real numbers. For virtual reactances higher than this threshold, one of the eigenvalues moves toward the right half plane, thus implying longer attenuation times. Thus, the SOFIE controllers offer the possibility of selecting a proper virtual reactance to improve the damping of the electromechanical modes. In general, the higher the reactance, the more damped the electromechanical modes are. However, it is not recommended to select values that exceed the threshold. Otherwise, the system may become too slow and, additionally, the angle stability may be compromised.

Besides, in Fig. 9 it can be observed how the variation of the virtual reactance plays also an important role in the location of the high frequency eigenvalues associated to the PLL of the SOFIE implementations. The higher the reactance, the lower the damping factor of these eigenvalues. Consequently, these results suggest the need to achieve a trade-off in the selection of the virtual reactance to properly attenuate both electromechanical and PLL modes.

V. Impact of the PLL in the performance of the SOFIE control

The aim of this section is to provide a more in depth analysis of the impact of the PLL dynamics on the proposed SOFIE 2 and 3 implementations.

As mentioned previously, the gains of the PI regulator of the PLL are calculated using the Symmetrical Optimum method, which determines the controller constants based on the output filter time constant (τ_f), and on a factor a that determines the crossover frequency and sets the damping. The values of the PI gains can be obtained as [21].

$$k_{p_{pll}} = \frac{1}{a\ \tau_f\ \omega_b} \qquad k_{i_{pll}} = \frac{k_{p_{pll}}}{a^2\ \tau_f} \tag{26}$$

The filter time constant τ_f is proportional to the response time of the PLL; the smaller the value of τ_f, the faster can the PLL react under frequency variations. This phenomena can be clearly observed in Fig. 10, where the eigenvalues of the SOFIE 3 implementation are illustrated for different τ_f values. If τ_f is below a threshold, meaning that the PLL is slow, the electromechanical eigenvalues are displaced towards the right half-plane, and the response of the SOFIE controllers starts to diverge from that of the SM. However, when τ_f is above the threshold, and the PLL is fast enough, the PLL dynamics do not influence the electromechanical eigenvalues. This is an interesting feature of the proposed SOFIE 2 and 3 controllers that make it possible to decouple the dynamics of the electromechanical modes from those of the PLL loop. In this sense, these controllers are recommended for power systems that are weak in terms of inertia but allow the use of a fast PLL to improve the dynamics of the converter. Under these conditions, the PLL eigenvalues have an attenuation constant significantly higher than that of the electromechanical modes and do not play a significant role in the dynamic response of the SOFIE controllers. Consequently, SOFIE controllers approximate the dynamic operation of SM properly.

Fig. 11 (a) depicts the time-domain waveforms of the active power of the SOFIE 3 controller for different values of τ_f under a -0.01 p.u. grid frequency variation and compares them

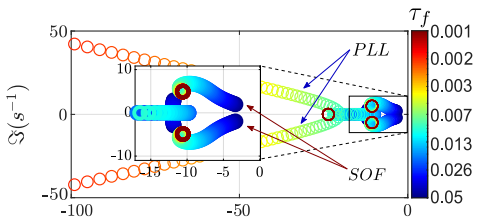

Fig. 10. Root-locus under a variation of the time constant (T_f).

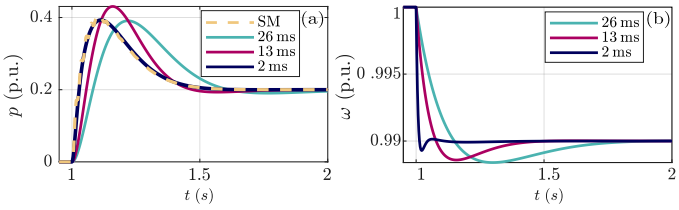

Fig. 11. SOFIE 3 performance under a −0.01 p.u. grid frequency variation for different τ_f values: a) Active power of the converter and the SM, b) Frequency estimated by the PLL and mechanical frequency of the SM.

against that of a SM. Alternatively, Fig. 11 (b) displays the frequency estimated by the PLL. The results reveal that when the PLL is fast, the SOFIE controller reproduces accurately the behaviour expected from a SM.

VI. Comparison of control SOFIE and SM in low inertia power system.

To study the dynamics of SOFIE control and its equivalence to a SM in a low inertia power system, the IEEE 9 test case shown in Fig. 12 is modelled [23]. The inverters and the SM have been connected to the grid via an *RL* series impedance ($Z_g = Z_c = 0.006 + 0.08j$). The SM is in charge of forming the grid and is modelled by a reduced-order system with a turbine and governor, as described in [10]. The parameters of the study can be found in Appendix A. Several studies have emphasised the need to use dynamic models to represent the transmission lines in converter-dominated networks, due to the adverse interaction that can take place between the converter and the lines and endanger the system's stability [24]. Thus, the transmission lines have been implemented as equivalent π models. The loads are implemented as constant *RL* impedances. In order to analyse the dynamic operation of the proposed control, the following case studies are proposed: i) inverters 1 and 2 are controlled with a classical droop control, but without inertia emulation (Droop case); ii) inverters 1 and 2 are equipped with SOFIE control (SOFIE case); iii) the inverters are replaced by the SM studied in the previous sections (SM case).

To analyse the inertial behaviour of the grid in the presence of power imbalances, a load variation of 0.05 p.u. at $t = 1$ s is applied at bus 6. Figure 13 shows how, when the converters do not provide emulated inertia (droop case), the grid frequency exhibits a significantly higher RoCoF and nadir. On the other hand, when the converters provide frequency support through the use of the SOFIE control, the system remains stable and their dynamic response matches accurately that of SMs', even for different inertia constants.

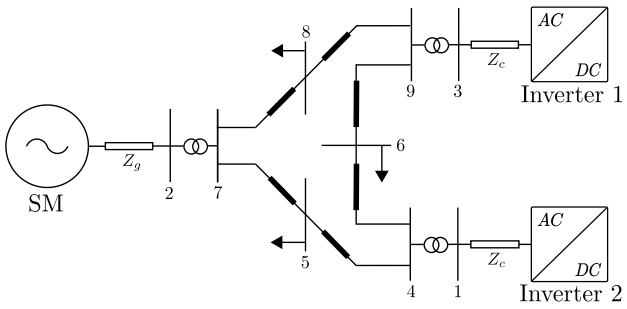

Fig. 12. Nine-bus power transmission system diagram [23].

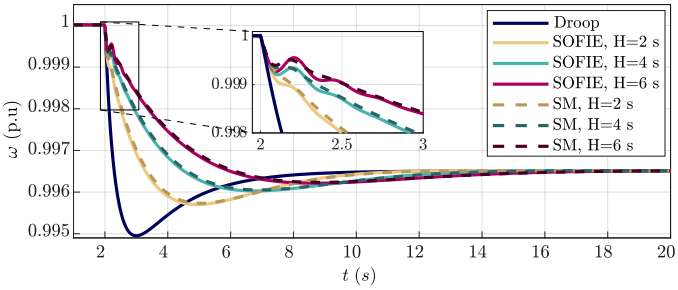

Fig. 13. Frequency behaviour under power imbalance, varying the inertia.

As mentioned above, one of the main challenges of the massive integration of converters into the power grid is the adverse interactions between the converter dynamics and the *LC* resonances of transmission lines. Therefore, to study these interactions, the eigenvalues of the nine-bus system are analysed. Figure 14 shows the root loci for the three proposed scenarios.

The eigenvalues associated to the electromechanical part are shown in the zoomed-in area. Outside the zoomed-in area are the modes associated with the resonances of the transmission lines.

The resonant modes in the droop case exhibit adverse interactions between the droop control and the transmission line resonances, causing these eigenvalues to move towards the right half plane. To achieve a stable point of operation the PLL speed has been reduced by setting the time constant as $\tau_f = 0.01$ (refer to Eq. (26)).

On the other hand, in the SOFIE case, the poles linked with the transmission line resonances remain in very similar positions compared to the SM scenario because the converter

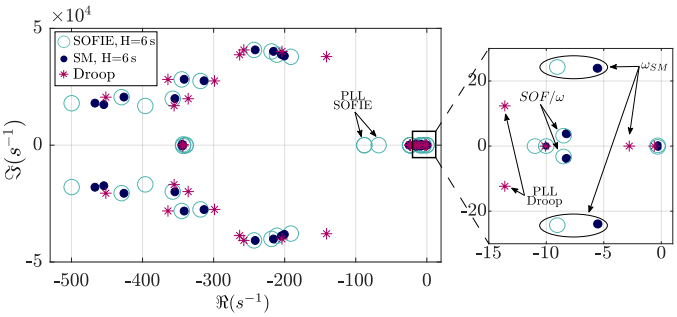

Fig. 14. Resonant and electromechanical modes behaviour.

dynamics do not interact with the passive components of the grid. This means that the SOFIE control keeps the system stability without exciting the modes associated with the *LC* resonances in a similar way to a SM in a traditional power system. It overcomes the stability drawbacks of classical GSCs based on droop control and first-order filter inertia emulation caused by interactions between the GSC control, the PLL and the *LC* resonances described in [12], [13].

VII. Experimental validation of SOFIE control

The aim of this section is to validate the performance of the proposed SOFIE implementations experimentally.

For that purpose, a hardware-in-the-loop (HIL) test bench based on an OPAL-RT is used (Fig. 15). The inverter semiconductors, inductive filter, grid-side impedance and the infinite bus have been has been emulated in the FPGA of the OPAL-RT. In contrast, the converter control comprised by the SOFIE implementation, the current reference calculator, the current controller, the PLL and the space vector modulator are implemented on a Texas Instruments TMS320F28379D. The validation is carried out following the same methodology as in Section III, which consists of testing the time domain performance of SOFIE implementations under varying network frequency (ω_g) in the system of the figure 3.

The results in Fig. 16 show that for a 0.01 p.u. variation in the active power reference, the experimental results match the dynamic response of the linearized models used to elaborate previous sections, thus validating them against a grid frequency variation. As mentioned previously, how the SOFIE 1 implementation has a higher power overshoot under sudden frequency variations compared to the other two variants. Additionally, it is also worth noting how the experimental results of the SOFIE 1 exhibit a significantly bigger noise than in the second and third configuration. This demonstrates the effectiveness of the second-order filter in the droop loop (refer to Fig. 1), since the frequency noise is not directly fed to the power controller. In SOFIE 2 and 3, the ripple is reduced to 0.02 p.u. compared to the 0.1 p.u. ripple of SOFIE 1.

Fig. 15. Opal-RT based real-time HIL testbed.

VIII. Conclusions

This paper presents a new grid-supporting control approach, with three different variants, that allows the converter to support the grid frequency while providing the equivalent inertial behaviour, primary response and damping of a SM. To validate whether the converter can reproduce the dynamics of a SM, time-based simulations and a detailed analysis of the eigenvalues of the system have been carried out. The results show how the proposed control implementations allow to a greater or lesser extent to operate a grid-connected converter with dynamics close to those of an ideal SM. Among the proposed implementations, SOFIE 3 is the approach that most accurately replicates the response of a simplified SM, while SOFIE 1 and SOFIE 2 require almost no variation on the structure of classical inertia emulation controllers, but replicate the operation of SMs with a lower degree of accuracy. Furthermore, the effect of the PLL has been analysed. If the PLL loop is fast enough, the dynamics of the dominant modes of the proposed SOFIE 2 and 3 controllers are decoupled from those of the PLL. It has been also shown how the faster the PLL, the closer the behaviour of the converter to that of a synchronous machine. The low inertia network study showed that SOFIE control emulates the inertial behaviour of an SM, improving the stability of converter-dominated systems without exciting the *LC* resonances of the grid. Experimental results have shown a good match with those of the analytical study, thus validating its main conclusions and the technical feasibility of the proposed SOFIE controllers.

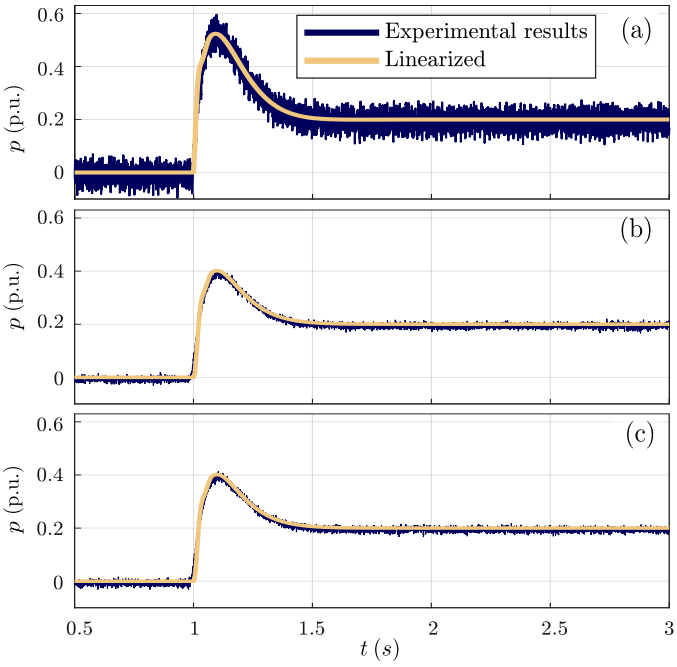

Fig. 16. Validation of the linearized model against real-time simulation based on Opal-RT in the face of a change of grid frequency. a) SOFIE 1 implementation, b) SOFIE 2 implementation, c) SOFIE 3 implementation.

Additionally, experimental results reveal that SOFIE 2 and 3 achieve considerable noise reduction.

All in all, SOFIE 2 implementation is recommended for applications where the dynamics of the power set-point should not be modified. This is the case, for instance, of the converter of a photovoltaic or wind generation system where the power set-point is calculated with a maximum power point tracking (MPPT) algorithm. On the other hand, the SOFIE 3 implementation is recommended for applications in which sharp changes in the power set-point require filtering to avoid sudden power transients.

References

[1] IRENA International Renewable Energy Agency, *Global Energy Transformation: A Roadmap to 2050*, 2019.

[2] B. K. Poolla, D. Groß, and F. Dörfler, "Placement and implementation of grid-forming and grid-following virtual inertia and fast frequency response," *IEEE Transactions on Power Systems*, vol. 34, no. 4, pp. 3035–3046, 2019.

[3] F. Milano, F. Dörfler, G. Hug, D. J. Hill, and G. Verbič, "Foundations and challenges of low-inertia systems (Invited Paper)," in *20th Power Syst. Comput. Conf. PSCC 2018*, 2018, pp. 1–25.

[4] R. Jadeja, A. Ved, T. Trivedi, and G. Khanduja, *Control of Power Electronic Converters in AC Microgrid*. Cham: Springer International Publishing, 2020, pp. 329–355.

[5] J. M. Guerrero, J. C. Vasquez, J. Matas, L. G. de Vicuna, and M. Castilla, "Hierarchical control of droop-controlled ac and dc microgrids–a general approach toward standardization," *IEEE Transactions on Industrial Electronics*, vol. 58, no. 1, pp. 158–172, 2011.

[6] E. Unamuno, J. A. Suul, M. Molinas, and J. A. Barrena, "Comparative Eigenvalue Analysis of Synchronous Machine Emulations and Synchronous Machines," in *IECON 2019 - 45th Annual Conference of the IEEE Industrial Electronics Society*. IEEE, oct 2019, pp. 3863–3870.

[7] S. D'Arco, J. A. Suul, and O. B. Fosso, "A Virtual Synchronous Machine implementation for distributed control of power converters in SmartGrids," *Electr. Power Syst. Res.*, vol. 122, pp. 180–197, 2015.

[8] G.-S. Seo, M. Colombino, I. Subotic, B. Johnson, D. Groß, and F. Dörfler, "Dispatchable virtual oscillator control for decentralized inverter-dominated power systems: Analysis and experiments," in *2019 IEEE Applied Power Electronics Conference and Exposition (APEC)*, 2019, pp. 561–566.

[9] T. Jouini, C. Arghir, and F. Dörfler, "Grid-Friendly Matching of Synchronous Machines by Tapping into the DC Storage," *IFAC-PapersOnLine*, vol. 49, no. 22, pp. 192–197, 2016.

[10] D. A. Aragon, E. Unamuno, S. Ceballos, and J. A. Barrena, "Comparative small-signal evaluation of advanced grid-forming control techniques," *Electric Power Systems Research*, vol. 211, p. 108154, 2022.

[11] M. S. Golsorkhi and D. D. Lu, "A decentralized power flow control method for islanded microgrids using V-I droop," *22nd Iran. Conf. Electr. Eng. ICEE 2014*, no. Icee, pp. 604–609, 2014.

[12] D. Duckwitz and B. Fischer, "Modeling and Design of df/dt -Based Inertia Control for Power Converters," *IEEE J. Emerg. Sel. Top. Power Electron.*, vol. 5, no. 4, pp. 1553–1564, 2017.

[13] J. Are Suul and S. D'Arco, "Comparative analysis of small-signal dynamics in virtual synchronous machines and frequency-derivative-based inertia emulation," in *2018 IEEE 18th International Power Electronics and Motion Control Conference (PEMC)*, 2018, pp. 344–351.

[14] Z. Ahmad, J. Rueda, N. Kumar, E. Rakhshani, P. Palensky, and M. Meijden, "A power hardware-in-the-loop based method for fapr compliance testing of the wind turbine converters control," *Energies*, vol. 13, 10 2020.

[15] N.-B. Lai, A. Tarraso, G. Baltas, L. V. Marin Arevalo, and P. Rodriguez, "External Inertia Emulation Controller for Grid-following Power Converter," *IEEE Trans. Ind. Appl.*, vol. 9994, no. c, pp. 1–1, 2021.

[16] D. A. Aragon, E. Unamuno, S. Ceballos, and J. A. Barrena, "Second-order filter-based inertia emulation (sofie) for low inertia power systems—part 2: Analysis and comparative evaluation," *IEEE Transactions on Power Delivery*, in review.

[17] P. Kundur and N. Balu, *Power System Stability and Control*, ser. EPRI power system engineering series. McGraw-Hill, 1994.

[18] M. S. Alam, F. S. Al-Ismail, A. Salem, and M. A. Abido, "High-level penetration of renewable energy sources into grid utility: Challenges and solutions," *IEEE Access*, vol. 8, pp. 190 277–190 299, 2020.

[19] T. Kerdphol, F. S. Rahman, M. Watanabe, Y. Mitani, D. Turschner, and H.-P. Beck, "Enhanced virtual inertia control based on derivative technique to emulate simultaneous inertia and damping properties for microgrid frequency regulation," *IEEE Access*, vol. 7, pp. 14 422–14 433, 2019.

[20] S. D'Arco, J. A. Suul, and O. B. Fosso, "Automatic tuning of cascaded controllers for power converters using eigenvalue parametric sensitivities," *IEEE Transactions on Industry Applications*, vol. 51, no. 2, pp. 1743–1753, 2015.

[21] J. A. Suul, K. Ljokelsoy, and T. Undeland, "Design, tuning and testing of a flexible PLL for grid synchronization of three-phase power converters," in *2009 13th Eur. Conf. Power Electron. Appl.*, 2009, pp. 1–10.

[22] D. Serrano-Jiménez, E. Unamuno, A. G. de Muro, D. Aragon, S. Ceballos, and J. Barrena, "Stability tool for electric power systems with a high penetration of electronic power converters," *Electric Power Systems Research*, vol. 210, p. 108115, 2022.

[23] P. Anderson, A. Fouad, I. of Electrical, E. Engineers, and I. P. E. Society, *Power System Control and Stability*, ser. IEEE Press power engineering series Power system control and stability. Wiley, 2003.

[24] U. Markovic, O. Stanojev, P. Aristidou, E. Vrettos, D. S. Callaway, and G. Hug, "Understanding Small-Signal Stability of Low-Inertia Systems," *IEEE Trans. Power Syst.*, p. 1, 2021.

Appendix

A. Parameter values

Table I shows the general system parameters and converter control loop parameters used in this study.

TABLE I
Parameter values for each case study.

System general values					
S_b	2.75 MVA	$v_{b_{ll-rms}}$	690 V	ω_b	$2\pi 50$ rad/s
Stiff grid					
L_g	0.03 p.u.	R_g	0.01 p.u.	ω_g^*	1 p.u.
Synchronous machine					
S	1 p.u.	L_s	0.27 p.u.	R_s	0.006 p.u
k_d	141	k_ω	20	H	3.50 s
Converter					
S	1 p.u.	L_f	0.08 p.u	R_f	0.006 p.u.
f_{sw}	2.12 kHz				
Control set-points					
p^*	0 p.u.	Q^*	0 p.u.	ω^*, v_{dc}	1 p.u.
Inner Current loop					
k_{pc}	0.54	k_{ic}	12.72	k_{ffv}, k_{xc}	1
SOFIE					
k_d	141	H	3.50 s	k_ω	20
X_s	0.03	ω_n	12.23 rad/s	ζ_v	0.94
$k_{p_{pll}}$	0.53	$k_{i_{pll}}$	29.47	τ_f	0.002 s
Low inertia power system (Sec. VI)					
SM (connected at bus 2)					
H	1 s	k_{ω_g}	4	k_{d_g}	0
t_T	1 s	t_G	0.1 s	k_v	0.1
SM (connected at buses 1 and 3)					
L_s	0.3 p.u.	R_s	0.006 p.u.	H	2, 4, 6 s
k_d	206	k_ω	4		
SOFIE					
k_d	206	H	2, 4, 6 s	k_ω	4
X_s	0.30	ω_n	9.34 rad/s	ζ_v	0.94
$k_{p_{pll}}$	0.53	$k_{i_{pll}}$	29.47	τ_f	0.002 s